Dose discrepancies in the buildup region and their impact on dose calculations for IMRT fields

Shu-Hui Hsu,[a] Jean M. Moran,[b] Yu Chen,[c] Ravi Kulasekere,[d] and Peter L. Roberson[e]
Department of Radiation Oncology, University of Michigan, Ann Arbor, Michigan 48109

(Received 8 October 2009; revised 10 March 2010; accepted for publication 12 March 2010; published 14 April 2010)

Purpose: Dose accuracy in the buildup region for radiotherapy treatment planning suffers from challenges in both measurement and calculation. This study investigates the dosimetry in the buildup region at normal and oblique incidences for open and IMRT fields and assesses the quality of the treatment planning calculations.
Methods: This study was divided into three parts. First, percent depth doses and profiles (for 5×5, 10×10, 20×20, and 30×30 cm^2 field sizes at 0°, 45°, and 70° incidences) were measured in the buildup region in Solid Water using an Attix parallel plate chamber and Kodak XV film, respectively. Second, the parameters in the empirical contamination (EC) term of the convolution/superposition (CVSP) calculation algorithm were fitted based on open field measurements. Finally, seven segmental head-and-neck IMRT fields were measured on a flat phantom geometry and compared to calculations using γ and dose-gradient compensation (C) indices to evaluate the impact of residual discrepancies and to assess the adequacy of the contamination term for IMRT fields.
Results: Local deviations between measurements and calculations for open fields were within 1% and 4% in the buildup region for normal and oblique incidences, respectively. The C index with 5%/1 mm criteria for IMRT fields ranged from 89% to 99% and from 96% to 98% at 2 mm and 10 cm depths, respectively. The quality of agreement in the buildup region for open and IMRT fields is comparable to that in nonbuildup regions.
Conclusions: The added EC term in CVSP was determined to be adequate for both open and IMRT fields. Due to the dependence of calculation accuracy on (1) EC modeling, (2) internal convolution and density grid sizes, (3) implementation details in the algorithm, and (4) the accuracy of measurements used for treatment planning system commissioning, the authors recommend an evaluation of the accuracy of near-surface dose calculations as a part of treatment planning commissioning.
[DOI: 10.1118/1.3377769]

Key words: electron contamination, convolution, surface dose, IMRT field, oblique incidence

I. INTRODUCTION

The determination of dose in the buildup region is an important issue for radiotherapy of near-surface targets, such as in the treatment of head-and-neck cancer or breast cancer. Because target volumes can be close to or extend to the skin, the skin dose or near-surface tumor dose must be accurately estimated to avoid unnecessary skin reactions or underdosing of near-surface target subvolumes. The accuracy of buildup dose suffers from the challenges in both calculations and measurements.

Many publications have reported accuracy for various treatment planning algorithms.[1–7] Dose disagreement at near-surface depths has been found with a range of variation in these studies. For example, Dogan *et al.*[5] studied the buildup dose for oblique IMRT beams using a parallel plate chamber and EDR2 film in a flat phantom. They used the FOCUS convolution/superposition algorithm to calculate the dose, and found that the calculated doses at the surface and 1 mm below the surface were overestimated by 25% and 5%, respectively, for the 0° incident $IMRT^{strip}$ beam (six static 1×6 cm^2 strips). Chung *et al.*[4] measured the buildup dose for IMRT using radiochromic film in a head-and-neck phantom. They found that PINNACLE and CORVUS treatment planning systems (TPSs) overestimated the surface dose for both shallow and deep target cases by 7.4%–18.5% with respect to the prescribed dose. Ramsey *et al.*[3] measured the buildup dose from helical tomotherapy using TLD and EDR2 film in an anthropomorphic phantom, and found that the calculated surface doses using HI-ART TPS were overestimated between 3% and 13%.

The sources of the buildup dose are complex and machine configuration dependent, including the primary photon beam, backscattered radiation from the patient, and contamination radiation from accelerator head and air volume. Because of the complexity of the source of buildup dose, an electron contamination model is usually added to the photon dose calculation model for model-based calculation algorithms to account for the dose contributed by contamination radiation in the buildup region.[8–11] Electron contamination could be directly measured or indirectly derived by subtracting the calculated depth dose with photon only from the measured depth dose.[12,13] Magnitude of contamination radiation dose depends on machine head configuration, energy, depth, field

size, field shape, air gap, and incident angle.[12–19] Therefore, the accuracy of the buildup dose calculation strongly depends on the accuracy of the electron contamination model for various irradiation conditions.

Monte Carlo (MC) methods have the potential to simulate physics interactions and provide more accurate dose information compared to model-based calculation algorithms. The MC must accurately model the configuration of the machine head and fully account for all contamination sources in the simulation in order to be able to provide accurate buildup doses. Discrepancies between measurements and MC calculations have been reported.[20,21] However, agreement for 6 MV can be reasonably good. Reported discrepancies at 6 MV are in the range of 3%–4% at 0.5 mm depth[20] or ~8% at 50 μm depth.[21] Discrepancies at higher energies can be much greater.[21–23] Contributors to discrepancies could be the perturbation caused by the presence of the measurement chamber[21] and imprecise description of the treatment head.[23] The accuracy of MC calculation in the buildup region remains questionable without better understanding of the sources of discrepancies.

To validate the accuracy of calculation algorithms in the buildup region, accurate dose measurement is necessary. However, it is difficult to measure the dose accurately in a region without charged particle equilibrium. The detectors typically used are the extrapolation ion chamber, parallel plate ion chamber, thermoluminescent dosimeter (TLD), diode, MOSFET, and radiochromic film.[5,7,15,24–31] In disequilibrium conditions, the placement of the detector inside the phantom causes electron fluence perturbations. These perturbations typically cause the detector to over-respond. An extrapolation ion chamber has been proposed as a suitable detector for measurements in the buildup region because the fluence perturbation can be minimized by the extrapolation method.[32] For evaluation of perturbation factors, the MC method can be used to investigate the perturbation correction and improve measurement accuracy.[21] Because the use of the extrapolation chamber is time consuming, a parallel plate ion chamber is usually used and corrected with empirical over-response correction factors for buildup dose measurements. Several studies reported the characteristics of parallel plate ion chambers, and showed that the chambers over-respond in the buildup region when compared to extrapolation chamber measurements. The magnitude of the over-response depends on energy, field size, chamber design, and incident angle, and is more pronounced at lower energies.[25,33–35]

Based on previous reports, the uncertainty of calculated dose in the buildup region does not solely depend on the performance of the calculation algorithm, but also depends on commissioning procedures for buildup region dosimetry, calculation parameters used for routine calculations, complexity of the treatment plan, etc. Thorough evaluation of the calculation algorithm would be helpful for proper interpretation of skin or near-surface tumor doses. To thoroughly evaluate the performance of a TPS (either MC methods or model-based algorithms), the dose information along central axis and off-axis must be acquired for simple and complex irradiation conditions. Therefore, this study was designed to investigate the dosimetry in the buildup region for open and IMRT fields for normal and oblique incidences. It is divided into three parts: (1) Measuring the central axis and off-axis doses in the buildup region for a range of field sizes and incident angles; (2) validating the calculation accuracy along the central axis and off-axis regions in the buildup region and improving the dose fits in the empirical contamination (EC) term of the convolution/superposition (CVSP) calculation algorithm for open fields; and (3) evaluating the impact of residual discrepancies and assessing the adequacy of the contamination term for IMRT fields.

II. MATERIALS AND METHODS

II.A. Phantom and measurement setup

An Attix parallel plate chamber (RMI Model 449, Middleton, WI) and Kodak X-OMAT V film (Eastman Kodak, Rochester, NY) with Solid Water phantom slabs (Gammex RMI Model 457, Middleton, WI) were used for the superficial dose measurements. The lateral dimensions of the phantom slabs were 30×30 or 40×40 cm^2 with thicknesses of 2 mm–5 cm. The slab phantoms were set at 90 cm source-to-surface distance (SSD). A minimum of 10 cm backscatter was used for all measurements. All measurements were performed with a 6 MV x-ray beam, dose rate of 400 MU/min, jaw only fields (MLC parked), and using a Varian 21EX linear accelerator (Varian, Palo Alto, CA) equipped with a Millennium 120 leaf MLC. The accelerator was calibrated with an output of 0.8 cGy/MU at a depth of 10 cm in water for a 10×10 cm^2 field size at 90 cm SSD (calibration point).

II.B. Measurements of percent depth dose (PDD) in the buildup region

The Attix chamber (1 mm electrode gap, 12.7 mm diameter collector, 13.5 mm guard ring width, 4.8 mg/cm^2 entrance window thickness, fitted in machined Solid Water slab) was used for PDD measurements because it has minimal polarity effect ($<$3.5% at all depths for 10×10 cm^2 field) and minimal over-response ($<$1% for 0° incidence) in the buildup region and can measure the dose near the surface.[34] The doses were measured along the central axis for field sizes of 5×5, 10×10, 20×20, and 30×30 cm^2, for incident angles of 0°, 45°, and 70°, and at several depths (0°: 0.2, 0.5, 1.0, 1.5, and 10 cm; 45°: 0.3, 0.6, 0.7, 1.0, 1.4, 5, and 10 cm slant depth; 70°: 0.6, 0.9, 1.2, 1.5, 5, 9.9, and 10.2 cm slant depth) (Fig. 1). The number of monitor units (MUs) was 100 for all measurements with the Attix chamber. The accumulated charge was measured with a Therapy Dosimeter Model 35040 electrometer (Chesterland, OH). A total of six readings for two bias voltages (+300 and −300 V) were acquired and averaged. The PDDs were obtained by normalizing the dose at measured depths to the dose at 10 cm (slant) depth for individual incident angles and field sizes.

To correct the over-response for the Attix chamber in the buildup region, a modified version of the Rawlinson equations[35] was used. The modified equations incorporate

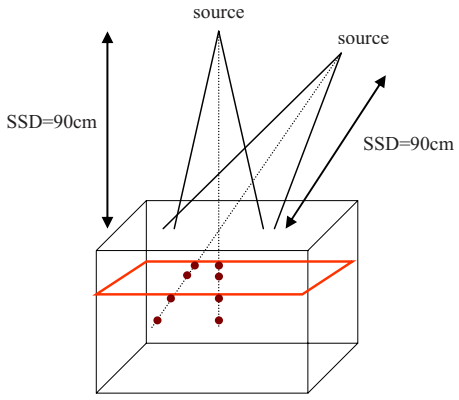

FIG. 1. Measurement diagram. The SSD was 90 cm for all incident angles and the PDDs were measured along the central axis of the beam.

the influence of oblique incidences based on the data reported by Gerbi *et al.*[25,33,34] The over-response correction factors for 6 MV x-rays were determined to be 0.7%, 2.3%, and 4.2% (relative to maximum dose D_{max}) at the surface for 0°, 45°, and 70° incident angles, respectively. For easier comparison with calculation, D_{max} normalization was converted to D_{10} (dose at 10 cm depth) normalization for these correction factors.

II.C. Measurements of profiles in the buildup region

For measurements using XV film, crossplane profiles (along the direction of leaf motion) were measured at several depths (0°: 0.2, 0.5, 1.5, 5, and 10 cm; 45°: 0.3, 0.6, 1.4, 5, and 10 cm slant depth; 70°: 0.6, 0.9, 1.5, 5, and 9.9 cm slant depth) for field sizes of 5×5 and 10×10 cm^2 and for incident angles of 0°, 45°, and 70°. The films were placed parallel to the phantom surface (Fig. 1) and irradiated to ~80 cGy to the central axis point on the film. The numbers of MUs used for exposure were adjusted based on PDDs from the Attix chamber for different incident angles, field sizes, and depths. To improve the accuracy of dose determination, dynamic calibration curves specific for each field size, depth, and incident angle were applied. All films were developed using a Kodak X-OMAT 3000RA Processor (Eastman Kodak, Rochester, NY), digitized with a Lumiscan75 (Lumisys, Sunnyvale, CA), and analyzed using in-house software. The film resolution was 0.15×0.15 mm^2. To quantify differences between profiles in the buildup region, the radiological width ($R50$) and the distance between 20% and 80% dose point in the penumbra region were calculated, relative to the dose at central axis for 0° incidence. For oblique incidences, the slope of the profile was considered in the determination of $R50$ and penumbra width.

II.D. CVSP algorithm

The superficial dose calculation was performed using the University of Michigan treatment planning system (UMPlan) and the CVSP algorithm[36] with an EC term.[37] The EC term supplements the dose along the central axis using an exponential term with an inplane-crossplane Gaussian blurring edge function. The exponential term is described by a maximum (EC_{MAX}) and linear attenuation factor (μ_{EC}) [Eq. (1)]. The Gaussian blurring edge function is described by standard deviations (σ_{EC_inside} and $\sigma_{EC\_outside}$). Parameters are different for large ($>15\times15$ cm^2) and small field sizes ($\leq15\times15$ cm^2).

$$EC(d) = EC_{MAX}\cdot F(\sigma_{EC\_inside},\sigma_{EC\_outside})\cdot e^{-\mu_{EC}\cdot d}, \quad (1)$$

where d is depth, EC_{max} is the contamination at surface, $F(\sigma_{EC\_inside},\sigma_{EC\_outside})$ is a Gaussian edge function of σ_{EC_inside} and $\sigma_{EC\_outside}$, and μ_{EC} is an attenuation factor with depth. In addition, a multiplicative flatness correction function is used for large fields only. The EC term is dependent on depth, off-axis distance, field size, and energy. IMRT fields are constrained to use small field parameters.

The field size dependence of the EC term is illustrated in Fig. 2. The Gaussian blurring edge function not only changes the magnitude in the off-axis region, but also changes the magnitude at central axis [Eq. (1)]. If the field size is much greater than $2\cdot\sigma_{EC\_inside}$, then the magnitude at central axis is

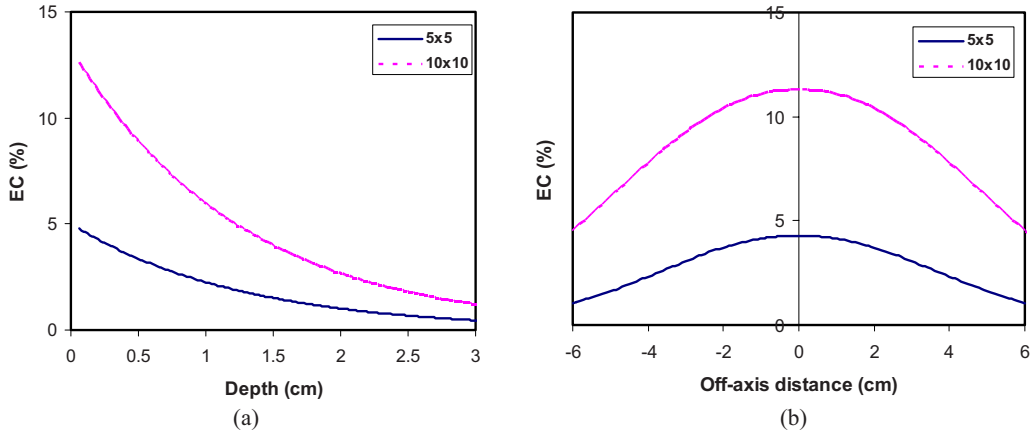

FIG. 2. An example of EC term for 5×5 and 10×10 cm^2 field sizes and 0° incidence in CVSP algorithm (a) along the central axis and (b) in crossplane direction (perpendicular to the beam axis) at 2 mm depth. The EC dose is relative to the dose at 10 cm depth for 10×10 cm^2 field size and 0° incidence (calibration point). EC term parameters are $EC_{MAX}=17.6\%$, $\mu_{EC}=0.78$ cm^{-1}, and $\sigma_{EC\_inside}=\sigma_{EC\_outside}=3.5$ cm.

not affected by the blurring edge function but the magnitude decreases when approaching a field edge. If the field size is comparable to or less than $2\cdot\sigma_{EC\_inside}$, the magnitude at central axis is decreased due to the blurring edge function and the magnitude still decreases further when approaching the field edge. The 10×10 cm^2 field ($>2\cdot\sigma_{EC\_inside}$) has a small reduction at central axis, while the 5×5 cm^2 field ($<2\cdot\sigma_{EC\_inside}$) is substantially reduced (Fig. 2).

The density, internal convolution, and calculation grid sizes also affect the accuracy of buildup dose calculation. The density grid includes all density information acquired from the anatomical images and its size depends on the scan acquisition geometry, e.g., the CT image pixelization and the space between CT slices. For an ideal homogeneous (water) phantom, the density grid size has a significant effect near the surface region only. The internal convolution grid is placed parallel and perpendicular to the beam axis. The densities for this grid are obtained through interpolation of the density grid data. The internal convolution grid size depends on the field size and phantom geometry. The calculated dose in the internal convolution grid for each beam is transformed into the dose in the calculation grid so that the dose in all beams can be accumulated. In this work, all three grid parameters were set as small as practical (typically 1 mm).

The PDDs and profiles were calculated for the smaller field sizes (5×5 and 10×10 cm^2) and all incident angles (0°, 45°, and 70°) at 90 cm SSD on a flat phantom with an internal convolution grid resolution of $1\times1\times1$ to $2\times2\times2$ mm^3, depending on the field size and incident angle. The calculation and density grid sizes were ~1 mm. The calculations were compared to measurements, and then the EC term parameters were adjusted, giving preference to agreement with the normal incidence data using an internal convolution grid size of 1 mm along the beam axis direction. The parameters in the EC term were acquired through fitting the EC exponential equation [Eq. (1)] to the measured dose less the calculated dose with photon only along the central axis in the buildup region for 5×5 and 10×10 cm^2 field sizes at 0° incidence using nonlinear least square method. Then, the agreement in the off-axis profiles inside the fields was checked and the $\sigma_{EC\_outside}$ parameter was manually tuned to fit off-axis measured profiles outside the fields.

II.E. IMRT fields

Seven segmental IMRT fields were randomly selected from four head-and-neck patient treatment plans. The constraints for leaf sequencing, using step-and-shoot MLC delivery based on the method of Bortfeld,[38] were number of segments (with maximum of 250) and 1% (of calculation maximum) fluence intervals with a 50% fluence offset. Field size or monitor unit constraints were not used. The total number of segments of each IMRT field varied from 127 to 285. Three of seven fields were split fields. The dose distributions of seven IMRT fields with beamlet size of 1×1 cm^2 were measured using XV film at 0.2, 0.5, 1.5, and 10 cm depths for 0° incidence and 90 cm SSD. The dose distributions of oblique incidences (45°: 0.3, 0.6, and 1.4 cm and 70°: 0.6, 0.9, and 1.5 cm) were measured for two IMRT fields out of the seven IMRT fields. Calibration curves for 5×5 cm^2 field size at different depths and angles were used to convert the film response to dose. All IMRT fields were recalculated with the new fit parameters under the same measurement condition with an internal convolution grid size between $1\times1\times1$ and $2\times2\times2$ mm^3.

To quantify the agreement between film measurements and calculations, dose-gradient compensation (C) index[39,40] was calculated with criteria of 2%/1 mm and 5%/1 mm [dose difference tolerance of maximum dose (%) and distance parameter (mm) for the gradient compensation]. For comparison, the γ index[41] was calculated with criteria of 2%/2 mm and 3%/3 mm [dose difference tolerance of maximum dose (%) and distance-to-agreement (mm)]. The percentage of points in agreement ($|C|,|\gamma|\leq1$) was calculated for the region where the dose was higher than 10% of maximum dose of the measurement [i.e., region of interest (ROI) is the dose >10% of maximum measured dose]. The C index with minimal gradient compensation (distance parameter of 1 mm) was chosen to focus the analysis on dose level discrepancies. Using both a tight (2%) and a loose (5%) dose criteria allows discrimination of the quality of the data-to-calculation comparison of near-surface IMRT dose distributions compared to IMRT dose distributions at a reference (10 cm) depth. Similarly, 2%/2 mm and 3%/3 mm criteria were chosen to represent the tight and loose criteria for the γ index. In addition to the use of C and γ indices to quantify the agreement, the average deviation for each IMRT field was calculated and represented the difference relative to the maximum of the measurement (for ROI > 10% of maximum measured dose).

II.F. Uncertainty analysis

The estimated uncertainty of Attix chamber measurement in the buildup region is 2% (one standard deviation, 1σ), including reading variation, error of geometric setup, and over-response correction. The estimated uncertainty of XV film measurements for open fields and IMRT fields is 2%, including geometric setup error and the use of depth-specific dynamic calibration curves.

III. RESULTS AND DISCUSSION

III.A. Measurement vs calculation for percent depth doses

Figure 3 shows the PDDs (relative to dose at 10 cm depth for individual field size and incident angle) in the buildup regions for field sizes of 5×5, 10×10, 20×20, and 30×30 cm^2 at 0°, 45°, and 70° incidences. In order to compare with previous reports in the literature, the surface doses were recalculated relative to D_{max}. Results were 9.1%, 15.2%, 27.1%, and 36.9% for 5×5, 10×10, 20×20, and 30×30 cm^2 field sizes at 0° incidence, respectively. Our results are within 1% for 5×5 and 10×10 cm^2, and 3% for 20×20 and 30×30 cm^2 compared to the data reported by Mellenberg.[42] This discrepancy is probably due to varying contribution from head scatter, where larger differences for

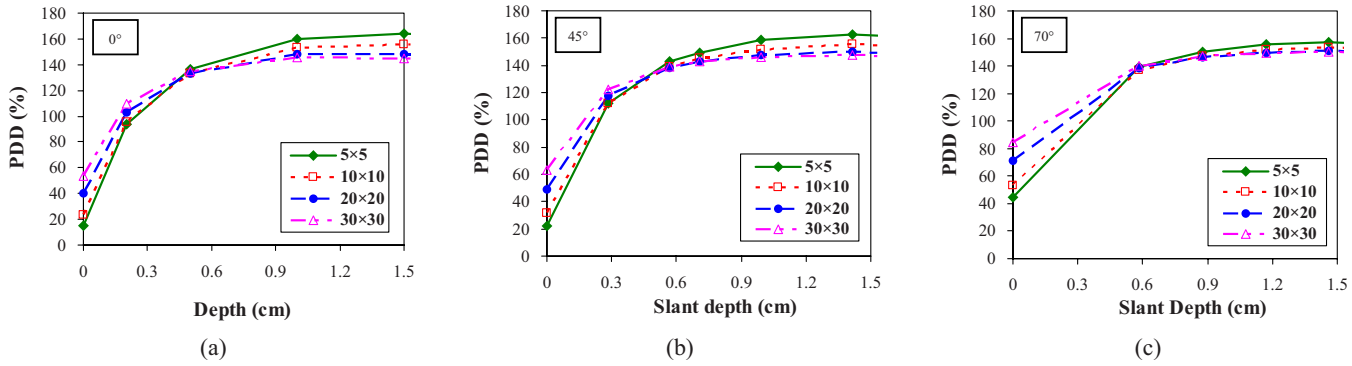

FIG. 3. PDDs for different field sizes at (a) 0°, (b) 45°, and (c) 70° using the Attix chamber. The PDDs are relative to 10 cm (slant) depth for individual field sizes and incident angles. Curves are to guide the eye only.

large fields are expected. Our result is also comparable to the surface doses summarized by Chiu-Tsao *et al.*[31] which range from 13% to 20% (excluding results from thicker TLDs) for 10×10 cm^2 field size at 6 MV photon beam.

The surface dose increases with increasing incident angle and field size. There are small increases in surface dose from 0° to 45° incidence, and rapid increases for larger incident angles. The angular dependence is similar for the four field sizes studied, largest at the surface and decreasing with increasing depth. The surface dose is approximately linearly dependent on the length of the side of the square field for the three incident angles. The surface dose dependence on incident angle and field size is similar to previous studies.[5,28,29,43,44] Due to the rapid increase in dose with angle of incidence, careful evaluation for the potential of skin toxicity should be performed for treatments with large angles of incidence.

Figure 4 compares PDDs between measurements and calculations to new fit parameters for 5×5 and 10×10 cm^2 field sizes at 0°, 45°, and 70° incidences. The dose shown in the figure is relative to the dose at the calibration point. The local deviation is percentage of the locally measured dose. The old EC term parameters were 36.7%, 1.8 cm^{-1}, 1.5 cm, and 3.5 cm for EC_{MAX}, μ_{EC}, σ_{EC_inside}, and $\sigma_{EC\_outside}$, respectively. The new EC term parameters were 17.6%, 0.78 cm^{-1}, 3.5 cm, and 3.5 cm for EC_{MAX}, μ_{EC}, σ_{EC_inside}, and $\sigma_{EC\_outside}$, respectively. The local deviation was reduced from 20% with the old fit parameters to 1% with the new fit parameters at 2 mm depth at 0° incidence. The local deviation with the new fit parameters is within 1% and 4% at 2 mm–1.5 cm depths for normal and oblique incidences, respectively. The deviation is largest for shallowest depth and largest incident angle. The average local deviation at depths from 2 mm to 1.5 cm is $0.5\%\pm1.1\%$. The calculation accuracy for oblique incidences is worse compared to normal incidence primarily because the parameters in the EC term were fitted to measured doses at 0° incidence.

The local deviation of surface dose (at zero depth) was large, up to 140% at 0° incidence for 5×5 cm^2 field size. Currently, it is impossible to decrease this discrepancy without deteriorating the agreement at other depths. However, the difference relative to the dose at the calibration point was between 12% and 25% for 5×5 and 10×10 cm^2 at 0°, 45°, and 70° incidences (see Fig. 4 insets). In addition, the dose at zero depth is not significant in clinical practice. The depths from 0.1 (epidermal thickness) to 2 mm (dermal thickness) are of most clinical concern for skin toxicity.[29,45] In this study, the calculation accuracy was estimated (through linear

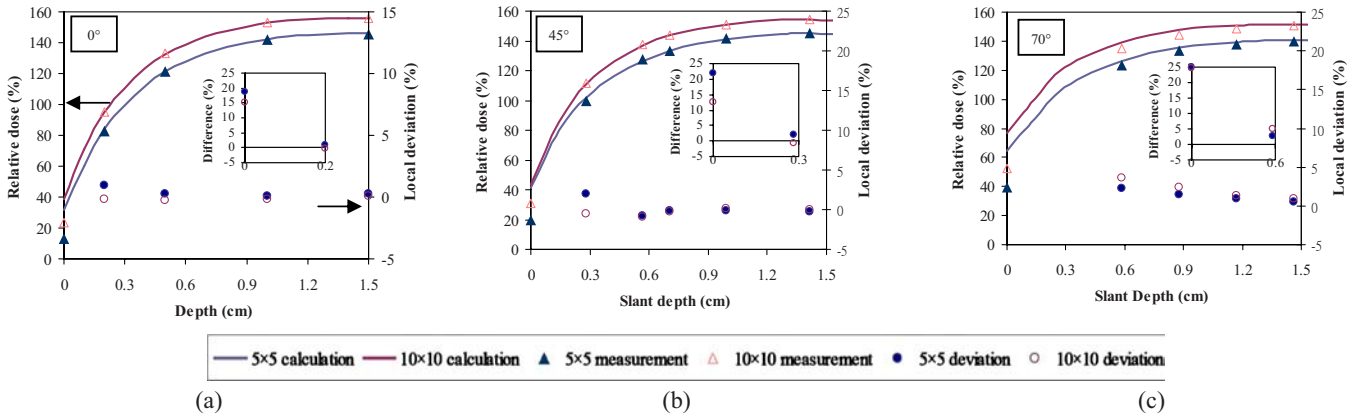

FIG. 4. Comparison of measured and calculated depth doses for 5×5 and 10×10 cm^2 fields at (a) 0°, (b) 45°, and (c) 70° incidences. The dose is relative to 10 cm depth for 10×10 cm^2 field at 0° incidence (calibration point) expressed in percent (%). The local deviation is percentage of the locally measured dose. Due to the large local deviation at the surface (up to 140%), the difference relative to the dose at the calibration point is shown in the insets.

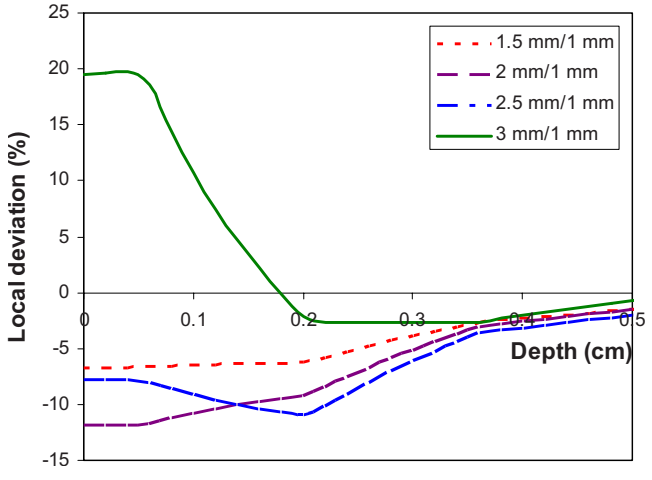

FIG. 5. The influence of internal convolution grid size (1 vs 1.5, 2, 2.5, and 3 mm) vs depth on the dose calculation for 10×10 cm^2 field size at 0° incident angle. The data were acquired through varying internal convolution grid size in the depth direction with constant size for other grids (e.g., internal convolution grid size in x and y directions and density grid size). The local deviation (%) is the relative difference between doses calculated with specified grid size and doses calculated with reference (1 mm) grid size. The local deviation is reduced to be within 2% beyond 5 mm depth. The behavior and magnitude of variation with internal convolution grid size is similar for 5×5 cm^2 field size.

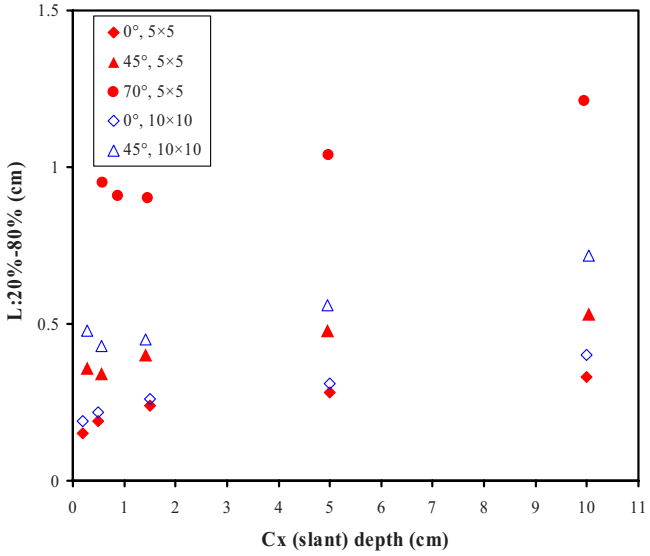

FIG. 6. The variation in 20%–80% left penumbra widths (in cm) with the depth along the central axis for 5×5 and 10×10 cm^2 field sizes and 0°, 45°, and 70° incident angles. For 70° incidence and 10×10 cm^2 field size, the film was too small to acquire the entire profile so the data are not shown here.

interpolation) to be within 10% (relative to the dose at the calibration point) at 1 mm depth for 0° incidence.

Some factors in the calculation setup were found to affect the accuracy in the buildup region. The calculated dose varies with internal convolution grid size in the depth direction. The effect of internal convolution grid size on the calculation is significant at depths shallower than 5 mm. Figure 5 shows the influence of internal convolution grid size (1, 1.5, 2, 2.5, and 3 mm) in the depth direction on the dose calculation as a function of depth shallower than 5 mm for 10×10 cm^2 field size at 0° incident angle. The difference is reduced to be within 2% at depths larger than 5 mm. In this study, the contamination term was fitted for the calculation with internal convolution grid size of 1 mm in the depth direction. Because of the strong dependence of internal convolution grid size, users must understand the limited accuracy at shallower depths due to grid size effects, possibly increasing the number of grid points when necessary or fitting the EC term with the clinically relevant grid size.

Attempts to validate MC calculation and measurement techniques for surface dose have been mixed, but tend to agree better at 6 MV compared to higher energies.[20–23] Abdel-Rahman *et al.*[21] found the discrepancy for a 6 MV photon beam was reduced from 26% to 8% (in local deviation) at 50 μm depth after simulating the configuration of the extrapolation chamber, while the discrepancy for an 18 MV photon beam was only reduced from 37% to 33%. Parsai *et al.*[20] reported a discrepancy of up to 3.6% at 0.5 mm depth for a 6 MV photon beam compared to extrapolation chamber measurements. Agreement between MC calculation and measurement in the buildup region depends on the accuracy of the treatment head simulation and on measurement chamber design and data interpretation.[46] Simple agreement is insufficient. A utility of the MC technique may be to understand the perturbation of detectors under disequilibrium conditions and to bolster confidence in surface dose measurement accuracy for a particular machine and detector setup.

III.B. Measurement vs calculation for profiles

Figure 6 shows the 20%–80% left penumbra widths at various depths for field sizes of 5×5 and 10×10 cm^2, and incident angles of 0°, 45°, and 70°. Left and right penumbras represent contralateral and ipsilateral sides relative to the gantry position for angled beams (left side and right side of Fig. 1, respectively). Generally, the penumbra width increases with increasing depth, field size, and incident angle. Comparing the measured $R50$ values and ideal $R50$ (geometric field at depth) for 0° incidence, the differences were within 1.5 mm. Discrepancies are attributed to measurement setup error and jaw position error.

Figure 7 shows measured and calculated profiles at shallow depths for 5×5 cm^2 at 0°, 45°, and 70° incidences, relative to the dose at the calibration point. The measured penumbra is slightly sharper than the calculated penumbra. The differences between measurements and calculations are within 1.8 and 1.2 mm for $R50$ and (left and right) penumbra widths, respectively. This difference has no significant dependence on the depth, field size, and incident angle. This difference was attributed to (1) the volume effect due to detector size when performing algorithm commissioning and (2) the larger internal convolution grid size (1×1 to 2×2 mm^2) compared to film measurement (0.15×0.15 mm^2). This discrepancy can be tolerated in the TPS.[47,48]

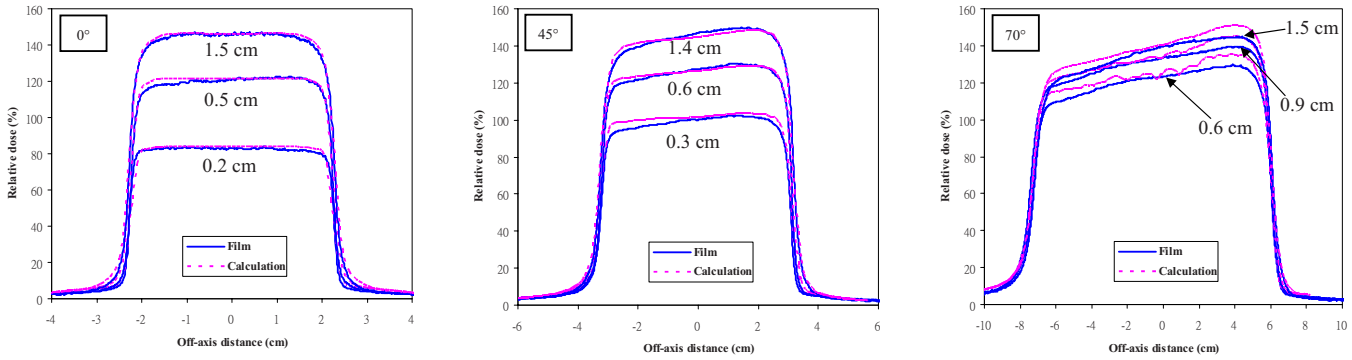

FIG. 7. The comparison of measured and calculated profiles in the buildup region for 5×5 cm^2 at (a) 0.2, 0.5, and 1.5 cm depths for 0° incidence; (b) 0.3, 0.6, and 1.4 cm slant depths for 45° incidence; and (c) 0.6, 0.9, and 1.5 cm slant depths for 70° incidence.

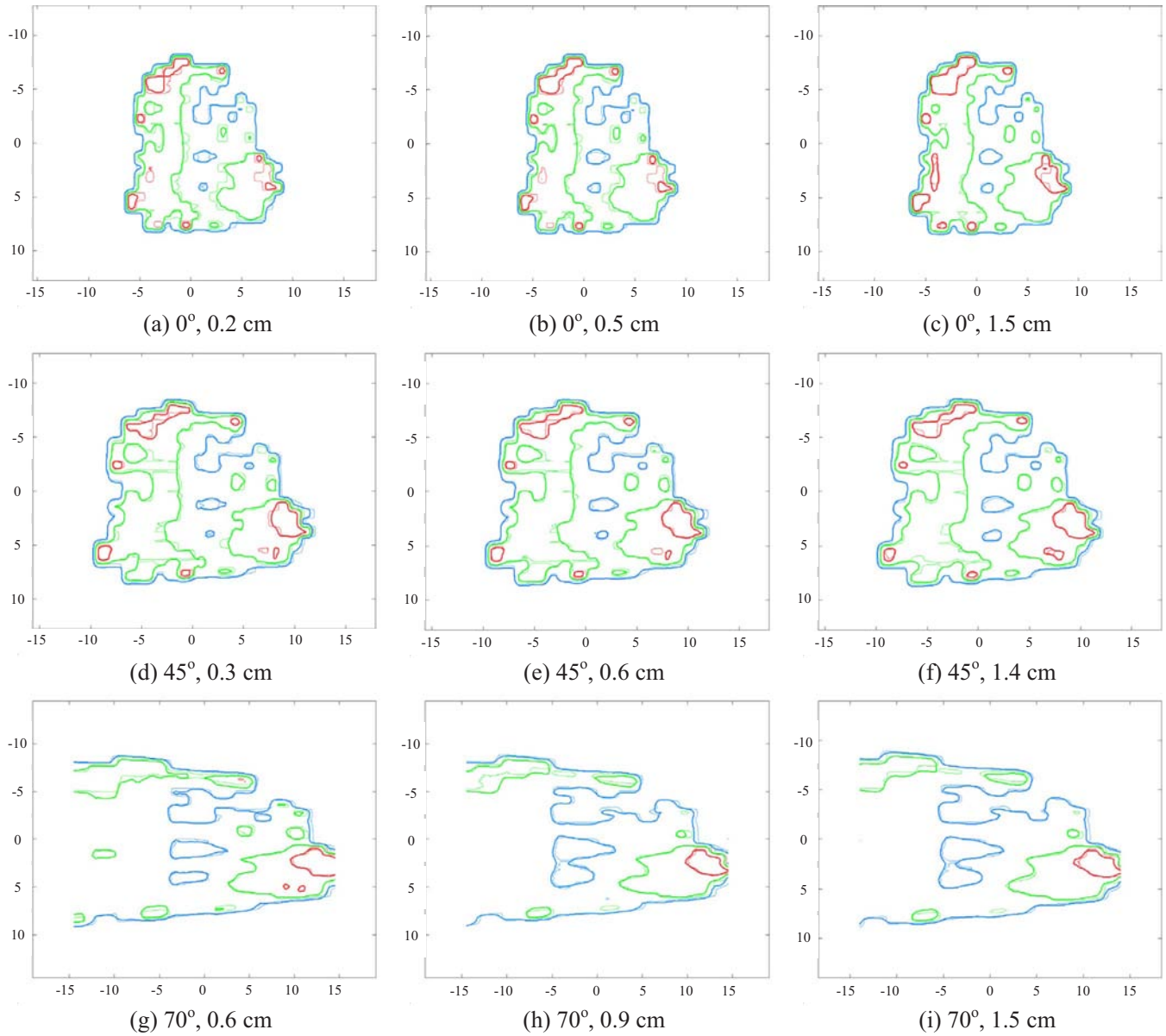

FIG. 8. The comparison of measured (thin lines) and calculated (bold lines) 2D dose distributions for IMRT field 1. Shown are [(a)–(c)] 0.2, 0.5, and 1.5 cm depths for 0° incidence; [(d)–(f)] 0.3, 0.6, and 1.4 cm slant depths for 45° incidence; and [(g)–(i)] 0.6, 0.9, and 1.5 cm slant depths for 70° incidence. For 70° incidence, the measurements were difficult to include entire fields so the figures shown are partial fields. The isodose lines are 20%, 50%, and 80% of maximum dose for each measurement. Total number of segments for this field was 284.

TABLE I. Comparison of film measurements and calculations for seven IMRT example fields at various depths for 0° incidence using γ index (2%/2 mm and 3%/3 mm) and C index (2%/1 mm and 5%/1 mm). Shown are percentages of points in agreement ($|\gamma|, |C| \leq 1$) for ROI > 10% of the maximum measured dose. Split field segment numbers are listed for each subfield. The average doses of calculations and measurements were acquired through averaging the doses for ROI > 10% of the maximum calculated dose and measured dose, respectively. The average deviation in percentage was calculated from averaging the ratio of dose difference (calculation minus measurement) to the maximum measured dose for all data points in ROI > 10% of the maximum measured dose.

						γ		C	
Field No	Depth (cm)	Segments	Calculation average dose (cGy)	Measurement average dose (cGy)	Average deviation (%)	2%/2 mm (%)	3%/3 mm (%)	2%/1 mm (%)	5%/1 mm (%)
1	0.2	183+101	30	33	−3.7	48	69	57	89
1	0.5	183+101	43	46	−2.8	61	85	71	95
1	1.5	183+101	50	50	0.9	89	97	90	99
1	10.0	183+101	30	30	0.5	84	95	86	98
2	0.2	237	32	32	−1.6	80	95	85	97
2	0.5	237	46	47	−1.6	82	96	86	97
2	1.5	237	54	52	1.7	79	91	82	96
2	10.0	237	32	29	1.4	76	89	78	96
3	0.2	127+149	18	19	−2.1	74	94	82	95
3	0.5	127+149	26	27	−1.8	83	97	86	97
3	1.5	127+149	30	29	0.8	89	97	89	99
3	10.0	127+149	17	17	1.4	82	94	84	97
4	0.2	152+133	21	23	−3.0	58	79	66	90
4	0.5	152+133	30	33	−2.6	66	87	73	94
4	1.5	152+133	36	35	1.0	84	95	85	97
4	10.0	152+133	22	21	1.3	83	93	83	97
5	0.2	155	30	31	−1.8	88	99	90	99
5	0.5	155	42	45	−2.1	86	99	90	99
5	1.5	155	49	51	0.9	91	99	92	100
5	10.0	155	30	28	1.8	82	93	82	98
6	0.2	189	28	29	−1.8	75	94	79	96
6	0.5	189	40	42	−1.8	83	98	86	97
6	1.5	189	47	46	1.3	87	97	86	98
6	10.0	189	28	26	1.3	85	95	84	97
7	0.2	127	19	19	−0.4	90	97	93	98
7	0.5	127	27	28	−0.8	93	98	94	98
7	1.5	127	31	30	2.0	70	88	75	97
7	10.0	127	19	17	2.7	66	84	72	97

Another discrepancy in Fig. 7 was the disagreement near the field periphery at shallow depths, especially for oblique incidences, where the calculated doses were larger than the measured doses (up to 5% local deviation). The primary cause is the inappropriate EC modeling in the off-axis region for oblique incidences when optimal fits were performed. The off-axis EC is symmetric at normal incidence but not at oblique incidences. The EC term contribution is also too high in the off-axis region for oblique incidences. Different modeling of the EC term would be necessary to achieve improved performance at all incident angles.

A main challenge in the profile comparisons was the ripple in the calculations for oblique incidences. The calculation ripples shown in Fig. 7(c) are irregular, appear at shallow depths, and disappear at a depth of D_{max} and beyond. The magnitude in the ripple was about 5%. The magnitude decreases with decreasing internal convolution grid spacing. The ripple is due to quantization near the phantom-air interface. For purposes of calculation, the phantom is subdivided into voxels based on the beam axis. The voxels near the surface are assigned densities based on averaging the density inside the voxel, which can include both air and phantom components. For oblique incidences, voxels are placed oblique to the phantom surface, resulting in nonsmooth densities and variations in SSD calculation for each surface voxel. Thus, the ripple phenomenon appears at shallow depths and increases the difficulty of determination of central axis dose. In addition to the internal convolution grid size, other factors which could affect the magnitude of ripple include the resolution of surface description and SSD calculation, calculation grid size, and density grid size. However, this ripple effect is less significant in patients' dosimetry due to nonflat surfaces and multiple beam incident angles. This effect can be minimized by modifying internal convolution grid and density grid parameters for an individual case.

III.C. Measurement vs calculation in IMRT fields

Seven segmental IMRT fields were tested using XV film on the flat phantom for normal and oblique incident angles. Figure 8 shows the comparison of one example field (field 1 from Table I) for normal and oblique incidences for 2D dose

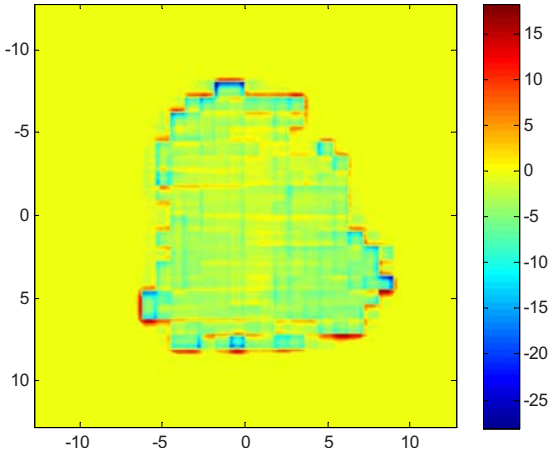

FIG. 9. An example of dose difference between calculation and measurement (calculation minus measurement) for IMRT field 1 at 2 mm depth and 0° incidence. The dose difference is -2.6 ± 3.4 cGy in average and 1σ. The maximum dose of the measurement is 69 cGy.

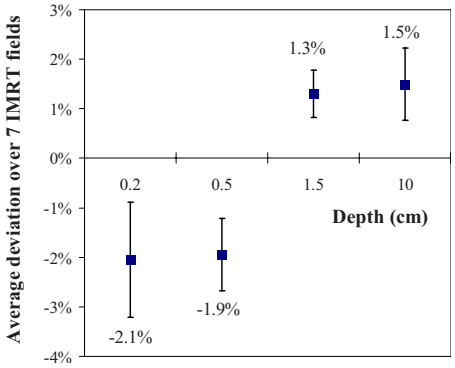

FIG. 10. The average of deviations between calculations and measurements for seven IMRT fields at various depths for 0° incidence (average value and 1σ shown).

distributions. The displayed isodose lines are 20%, 50%, and 80% of maximum dose on the measured dose maps. Figure 9 shows an example of dose difference (in cGy) map at 2 mm depth (field 1). The dose difference is -2.6 ± 3.4 cGy (average and 1σ).

To quantify the range of disagreement, the C index was used with criteria of 2%/l mm and 5%/l mm for the seven IMRT fields. For comparison, the γ index with criteria of 2%/2 mm and 3%/3 mm was also calculated. Table I shows the comparison at 0° incidence. The C index with 2%/1 mm (tight) criteria for IMRT fields ranged from 57% to 93% and from 72% to 86% at 2 mm and 10 cm depths, respectively. The C index with 5%/1 mm (loose) criteria for IMRT fields ranged from 89% to 99% and from 96% to 98% at 2 mm and 10 cm depths, respectively. Both tight and loose criteria in the C index show that the agreement in the buildup region is comparable to that at 10 cm depth. The γ index shows similar results. Table II shows the agreement in the buildup region for 45° incidence for selected fields. The agreement is also comparable to that at 0° incidence and 10 cm depth. Based on the results for 2D maps and the γ and C indices, the calculations agree well with the measurements in the buildup region for IMRT fields. The deviations found in the profiles for oblique incidences, i.e., disagreement near the profile edge and ripple phenomenon (Fig. 7), were partially masked in IMRT comparisons by dose nonuniformity effects.

Although the two indices show that the agreement is good, the calculated dose was found lower at 2 and 5 mm depths but higher at 1.5 cm and 10 cm depths (Fig. 10). A contributor to this systematic error could be measurement error, e.g., applying the calibration curves of open fields to IMRT fields. Errors in the calculation could also contribute to this systematic error because the irradiation geometry is not exactly represented by the calculation. The current EC term in the calculation algorithm does not consider the complexity of IMRT field delivery. Dogan *et al.*[5] and Yokoyama *et al.*[49] have shown that the dose at near-surface depth is lower for IMRT field delivery compared to open field delivery when the fluence pattern is the same. The reduction in dose at 2 mm depth is ~11% (relative to dose at 10 cm depth) for ten static 1×10 cm^2 strips compared to a 10×10 cm^2 open field.[49] Irradiation conditions are different between the fluence pattern used for the calculation and IMRT delivery fields with varying MLC shape patterns created during leaf sequencing. A small buildup dose discrepancy caused by ignoring the MLC shape patterns in the calculation was expected and may depend on IMRT pattern complexity, but a dependence relationship could not be concluded from the limited number of studied fields in this work.

The parameters in the EC term could be fitted based on either open or IMRT field geometries or a median solution, depending on individual clinical concerns and TPS performance. In this study, we fitted the parameters to open field geometry at 0° incidence and evaluated the residual discrep-

TABLE II. Comparison of film measurements and calculations for two IMRT example fields at various depths for 45° incidence using γ and C analyses.

Field No.	Depth (cm)	Segments	Calculation average dose (cGy)	Measurement average dose (cGy)	Average deviation (%)	γ 2%/2 mm (%)	γ 3%/3 mm (%)	C 2%/1 mm (%)	C 5%/1 mm (%)
1	0.3	183+101	37	38	−1.3	70	87	74	92
1	0.6	183+101	45	46	−1.1	83	95	85	95
1	1.4	183+101	50	50	−0.2	81	94	83	96
3	0.3	127+149	22	23	−0.1	84	95	85	97

ancy for IMRT fields because near-surface dose is not only a concern for IMRT treatments but also for conventional non-IMRT treatments. Based on current results in studied irradiation conditions, the calculation accuracy in the buildup region is within 4% for open and IMRT fields at normal and oblique incidences. The added EC term in CVSP was determined to be adequate for both open and IMRT fields.

Further work on the verification of surface dose on a curved surface (e.g., cylindrical) phantom with the full IMRT plan could be done. The discrepancy between measurements and calculations would be small for the multiple angles of beam incidence relative to the phantom surface on the basis of current results in the flat phantom geometry.

Many publications have reported accuracy for various treatment planning algorithms.[1–7] Dose disagreement at near-surface depths has been found with a range of variation in these studies. The calculation accuracy at near-surface depth depends on institution TPS commissioning in the buildup region (e.g., accuracy of measurement and versatility of the TPS algorithm), the complexity of treatment planning, and the size of different types of grids. It is recommended that users evaluate the buildup dose accuracy for their TPS using clinically relevant treatment plans and grid size(s).

IV. CONCLUSIONS

The calculation accuracy in PDDs and profiles for open fields has been improved by refitting parameters in the EC term based on more accurate buildup dose measurements. The main challenges in fitting profile measurements were the disagreement near the profile penumbra and a ripple phenomenon due to internal convolution grid effects for oblique incidences. These challenges do not significantly affect routine IMRT dose calculations. The quality of agreement in the buildup region for IMRT fields is comparable to the quality of agreement in nonbuildup regions. The calculation accuracy in the buildup region is within 4% for open and IMRT fields at normal and oblique incidences based on the results in studied conditions. The added EC term serves the purpose of supplementing the dose in the near-surface regions with adequate accuracy. The accuracy of calculation in the buildup region depends on methods used to parameterize the calculation model for the TPS, the accuracy of the EC modeling for various complexities of treatment plan, and the size of different types of grids. It is recommended that users evaluate the accuracy in the near-surface dose calculation for individual TPS with treatment plans and grid sizes which are typically used in clinic. Understanding the performance and limitation for individual TPS in the buildup dose calculation would provide helpful information when dose estimation at near-surface depths is needed.

ACKNOWLEDGMENTS

The authors thank Dr. Benedick Fraass and Dr. Eduardo Acosta for valuable discussions. This work was supported by NIH Grant No. P01CA59827.

[a]Electronic mail: shuihsu@umich.edu
[b]Electronic mail: jmmoran@med.umich.edu
[c]Electronic mail: ychen7@gmail.com
[d]Electronic mail: ravi.kulasekere@uhhospitals.org
[e]Electronic mail: roberpl@med.umich.edu

[1]S. Mutic and D. A. Low, "Superficial doses from serial tomotherapy delivery," Med. Phys. **27**, 163–165 (2000).
[2]P. D. Higgins, E. Y. Han, J. L. Yuan, S. Hui, and C. K. Lee, "Evaluation of surface and superficial dose for head and neck treatments using conventional or intensity-modulated techniques," Phys. Med. Biol. **52**, 1135–1146 (2007).
[3]C. R. Ramsey, R. M. Seibert, B. Robison, and M. Mitchell, "Helical tomotherapy superficial dose measurements," Med. Phys. **34**, 3286–3293 (2007).
[4]H. Chung, H. Jin, J. F. Dempsey, C. Liu, J. Palta, T. S. Suh, and S. Kim, "Evaluation of surface and build-up region dose for intensity-modulated radiation therapy in head and neck cancer," Med. Phys. **32**, 2682–2689 (2005).
[5]N. Dogan and G. P. Glasgow, "Surface and build-up region dosimetry for obliquely incident intensity modulated radiotherapy 6 MV x rays," Med. Phys. **30**, 3091–3096 (2003).
[6]D. Cheek, J. P. Gibbons, I. I. Rosen, and K. R. Hogstrom, "Accuracy of TomoTherapy treatments for superficial target volumes," Med. Phys. **35**, 3565–3573 (2008).
[7]Z. Y. Qi, X. W. Deng, S. M. Huang, L. Zhang, Z. C. He, X. A. Li, I. Kwan, M. Lerch, D. Cutajar, P. Metcalfe, and A. Rosenfeld, "In vivo verification of superficial dose for head and neck treatments using intensity-modulated techniques," Med. Phys. **36**, 59–70 (2009).
[8]A. Van Esch, L. Tillikainen, J. Pyykkonen, M. Tenhunen, H. Helminen, S. Siljamaki, J. Alakuijala, M. Paiusco, M. Lori, and D. P. Huyskens, "Testing of the analytical anisotropic algorithm for photon dose calculation," Med. Phys. **33**, 4130–4148 (2006).
[9]M. Miften, M. Wiesmeyer, S. Monthofer, and K. Krippner, "Implementation of FFT convolution and multigrid superposition models in the FOCUS RTP system," Phys. Med. Biol. **45**, 817–833 (2000).
[10]G. Starkschall, R. E. Steadham, Jr., R. A. Popple, S. Ahmad, and I. I. Rosen, "Beam-commissioning methodology for a three-dimensional convolution/superposition photon dose algorithm," J. Appl. Clin. Med. Phys. **1**, 8–27 (2000).
[11]L. Cozzi, F. M. Buffa, and A. Fogliata, "Dosimetric features of linac head and phantom scattered radiation outside the clinical photon beam: Experimental measurements and comparison with treatment planning system calculations," Radiother. Oncol. **58**, 193–200 (2001).
[12]A. Lopez Medina, A. Teijeiro, J. Garcia, J. Esperon, J. A. Terron, D. P. Ruiz, and M. C. Carrion, "Characterization of electron contamination in megavoltage photon beams," Med. Phys. **32**, 1281–1292 (2005).
[13]T. C. Zhu and J. R. Palta, "Electron contamination in 8 and 18 MV photon beams," Med. Phys. **25**, 12–19 (1998).
[14]P. J. Biggs, A. L. Boyer, and K. P. Doppke, "Electron dosimetry of irregular fields on the Clinac 18," Int. J. Radiat. Oncol., Biol., Phys. **5**, 433–440 (1979).
[15]B. J. Gerbi, A. S. Meigooni, and F. M. Khan, "Dose buildup for obliquely incident photon beams," Med. Phys. **14**, 393–399 (1987).
[16]A. Lamb and S. Blake, "Investigation and modeling of the surface dose from linear accelerator produced 6 and 10 MV photon beams," Phys. Med. Biol. **43**, 1133–1146 (1998).
[17]P. L. Petti, M. S. Goodman, T. A. Gabriel, and R. Mohan, "Investigation of buildup dose from electron contamination of clinical photon beams," Med. Phys. **10**, 18–24 (1983).
[18]P. L. Petti, M. S. Goodman, J. M. Sisterson, P. J. Biggs, T. A. Gabriel, and R. Mohan, "Sources of electron contamination for the Clinac-35 25-MV photon beam," Med. Phys. **10**, 856–861 (1983).
[19]J. Yang, J. S. Li, L. Qin, W. Xiong, and C. M. Ma, "Modeling of electron contamination in clinical photon beams for Monte Carlo dose calculation," Phys. Med. Biol. **49**, 2657–2673 (2004).
[20]E. Ishmael Parsai, D. Shvydka, D. Pearson, M. Gopalakrishnan, and J. J. Feldmeier, "Surface and build-up region dose analysis for clinical radiotherapy photon beams," Appl. Radiat. Isot. **66**, 1438–1442 (2008).
[21]W. Abdel-Rahman, J. P. Seuntjens, F. Verhaegen, F. Deblois, and E. B. Podgorsak, "Validation of Monte Carlo calculated surface doses for megavoltage photon beams," Med. Phys. **32**, 286–298 (2005).
[22]G. X. Ding, "Dose discrepancies between Monte Carlo calculations and measurements in the buildup region for a high-energy photon beam,"

Med. Phys. **29**, 2459–2463 (2002).
[23]O. Chibani and C. M. Ma, "On the discrepancies between Monte Carlo dose calculations and measurements for the 18 MV Varian photon beam," Med. Phys. **34**, 1206–1216 (2007).
[24]S. Devic, J. Seuntjens, W. Abdel-Rahman, M. Evans, M. Olivares, E. B. Podgorsak, T. Vuong, and C. G. Soares, "Accurate skin dose measurements using radiochromic film in clinical applications," Med. Phys. **33**, 1116–1124 (2006).
[25]B. J. Gerbi and F. M. Khan, "Measurement of dose in the buildup region using fixed-separation plane-parallel ionization chambers," Med. Phys. **17**, 17–26 (1990).
[26]T. Kron, A. Elliot, T. Wong, G. Showell, B. Clubb, and P. Metcalfe, "X-ray surface dose measurements using TLD extrapolation," Med. Phys. **20**, 703–711 (1993).
[27]T. Kron, M. Butson, F. Hunt, and J. Denham, "TLD extrapolation for skin dose determination in vivo," Radiother. Oncol. **41**, 119–123 (1996).
[28]J. P. Lin, T. C. Chu, S. Y. Lin, and M. T. Liu, "Skin dose measurement by using ultra-thin TLDs," Appl. Radiat. Isot. **55**, 383–391 (2001).
[29]H. F. Xiang, J. S. Song, D. W. Chin, R. A. Cormack, R. B. Tishler, G. M. Makrigiorgos, L. E. Court, and L. M. Chin, "Build-up and surface dose measurements on phantoms using micro-MOSFET in 6 and 10 MV x-ray beams and comparisons with Monte Carlo calculations," Med. Phys. **34**, 1266–1273 (2007).
[30]K. S. Smith, J. P. Gibbons, B. J. Gerbi, and K. R. Hogstrom, "Measurement of superficial dose from a static tomotherapy beam," Med. Phys. **35**, 769–774 (2008).
[31]S.-T. Chiu-Tsao and M. F. Chan, "Photon beam dosimetry in the superficial buildup region using radiochromic EBT film stack," Med. Phys. **36**, 2074–2083 (2009).
[32]B. Nilsson and A. Montelius, "Fluence perturbation in photon beams under nonequilibrium conditions," Med. Phys. **13**, 191–195 (1986).
[33]B. J. Gerbi and F. M. Khan, "Plane-parallel ionization chamber response in the buildup region of obliquely incident photon beams," Med. Phys. **24**, 873–878 (1997).
[34]B. J. Gerbi, "The response characteristics of a newly designed plane-parallel ionization chamber in high-energy photon and electron beams," Med. Phys. **20**, 1411–1415 (1993).
[35]J. A. Rawlinson, D. Arlen, and D. Newcombe, "Design of parallel plate ion chambers for buildup measurements in megavoltage photon beams," Med. Phys. **19**, 641–648 (1992).
[36]T. R. Mackie, J. W. Scrimger, and J. J. Battista, "A convolution method of calculating dose for 15-MV x rays," Med. Phys. **12**, 188–196 (1985).
[37]B. A. Fraass and I. A. D. Bruinvis, "Calculation of accurate dose distributions in the buildup region of conformal fields using a simple model for electron contamination," in Proceedings of the 15th Annual European Society for Therapeutic Radiology and Oncology [Radiother. Oncol. **40**, S9 (1996)].
[38]T. R. Bortfeld, D. L. Kahler, T. J. Waldron, and A. L. Boyer, "X-ray field compensation with multileaf collimators," Int. J. Radiat. Oncol., Biol., Phys. **28**, 723–730 (1994).
[39]J. M. Moran, J. Radawski, and B. A. Fraass, "A dose gradient analysis tool for IMRT QA," J. Appl. Clin. Med. Phys. **6**, 62–73 (2005).
[40]Y. Chen, J. M. Moran, D. A. Roberts, Y. El-Mohri, L. E. Antonuk, and B. A. Fraass, "Performance of a direct-detection active matrix flat panel dosimeter (AMFPD) for IMRT measurements," Med. Phys. **34**, 4911–4922 (2007).
[41]D. A. Low, W. B. Harms, S. Mutic, and J. A. Purdy, "A technique for the quantitative evaluation of dose distributions," Med. Phys. **25**, 656–661 (1998).
[42]D. E. Mellenberg, Jr., "Determination of build-up region over-response corrections for a Markus-type chamber," Med. Phys. **17**, 1041–1044 (1990).
[43]K. Y. Quach, J. Morales, M. J. Butson, A. B. Rosenfeld, and P. E. Metcalfe, "Measurement of radiotherapy x-ray skin dose on a chest wall phantom," Med. Phys. **27**, 1676–1680 (2000).
[44]S. Stathakis, J. S. Li, K. Paskalev, J. Yang, L. Wang, and C. M. Ma, "Ultra-thin TLDs for skin dose determination in high energy photon beams," Phys. Med. Biol. **51**, 3549–3567 (2006).
[45]J. W. Hopewell, "The skin: Its structure and response to ionizing radiation," Int. J. Radiat. Biol. **57**, 751–773 (1990).
[46]I. J. Chetty, B. Curran, J. E. Cygler, J. J. DeMarco, G. Ezzell, B. A. Faddegon, I. Kawrakow, P. J. Keall, H. Liu, C. M. Ma, D. W. Rogers, J. Seuntjens, D. Sheikh-Bagheri, and J. V. Siebers, "Report of the AAPM Task Group No. 105: Issues associated with clinical implementation of Monte Carlo-based photon and electron external beam treatment planning," Med. Phys. **34**, 4818–4853 (2007).
[47]B. Fraass, K. Doppke, M. Hunt, G. Kutcher, G. Starkschall, R. Stern, and J. Van Dyke, "American Association of Physicists in Medicine Radiation Therapy Committee Task Group 53: Quality assurance for clinical radiotherapy treatment planning," Med. Phys. **25**, 1773–1829 (1998).
[48]J. Venselaar, H. Welleweerd, and B. Mijnheer, "Tolerances for the accuracy of photon beam dose calculations of treatment planning systems," Radiother. Oncol. **60**, 191–201 (2001).
[49]S. Yokoyama, P. L. Roberson, D. W. Litzenberg, J. M. Moran, and B. A. Fraass, "Surface buildup dose dependence on photon field delivery technique for IMRT," J. Appl. Clin. Med. Phys. **5**, 71–81 (2004).